Research Square

Preprints are preliminary reports that have not undergone peer review.
They should not be considered conclusive, used to inform clinical practice,
or referenced by the media as validated information.

Fiber Effects on Brittleness Mitigation in Marble Dust Concrete

Ibrahim Alameri

i.ameri@su.edu.ye

Sana'a University

Abdulmalek Al-Jolahy

Sana'a University

Ali A. Al-Kadas

Sana'a University

Abdulwahed A. Mohmmed

Sana'a University

Sulaiman Alsafi

Sana'a University

Research Article

Keywords: brittleness index, recycled PET fiber, marble dust, fiber, environmental efficiency, circular economy, waste valorization, sustainable concrete, life cycle assessment

Posted Date: November 4th, 2026

DOI: https://doi.org/10.21203/rs.3.rs-10706140/v1

License: This work is licensed under a Creative Commons Attribution 4.0 International License.
Read Full License

Additional Declarations: No competing interests reported.

Fiber Effects on Brittleness Mitigation in Marble Dust Concrete

Ibrahim Alameri[1], Abdulmalek Al-Jolahy[1], Ali A. Al-Kadas[1], Abdulwahed A. Mohmmed[1], Sulaiman Alsafi[1]

[1]*Department of Civil Engineering, Faculty of Engineering, Sana'a University, Sana'a, Yemen*

Corresponding Author: Ibrahim Alameri (i.ameri@su.edu.ye)

Abstract

Concrete brittleness limits its use in bending-dominated elements. It also raises the cost of tensile reinforcement. A three-stage experimental program was carried out to address this limitation while also reducing the environmental burden associated with clinker production. In Stage I, marble dust (MD) was used to replace Portland cement at five levels, from 5% to 14% of binder mass. A 10% replacement gave the highest 28-day compressive strength, 49.64 MPa, and the highest modulus of rupture, 6.18 MPa, at a w/b of 0.364. In Stages II and III, polypropylene macro-fibers (PP), recycled PET bottle strips (rPET), and hooked-end steel fibers (SF) were added to the MD10 mixture, across twelve dosages in total. The brittleness index was reduced by up to 27.3% relative to the unreinforced MD10 mixture, which had an index of 8.03. Recycled PET fibers at a 1.00% volume fraction gave the lowest brittleness index of any mixture tested, 5.84, lower than every steel-fiber dosage. A cost and carbon assessment was then carried out, using validated emission factors and regional material prices. It showed that rPET fibers achieved this reduction for a material cost premium of only 1.68 USD per cubic meter and a carbon overhead of 7.66 kg CO_2e per cubic meter. The resulting cost efficiency index, 0.77 USD/m^3 per unit of brittleness reduction, and environmental efficiency index, 3.50 kg CO_2e/m^3 per unit of brittleness reduction, were substantially lower: the corresponding value for the best performing steel fiber dosage were approximately 79 and 36 times lower higher, respectively. Recycled PET fibers in a marble dust matrix are therefore a structurally effective, low-cost, and low-carbon route to brittleness reduction in sustainable concrete.

Keywords: brittleness index; recycled PET fiber; marble dust; fiber; environmental efficiency; circular economy; waste valorization; sustainable concrete; life cycle assessment.

1. Introduction

Concrete is the most widely produced manufactured material. Annual output exceeds 10 billion tonnes. Clinker calcination releases about 0.83 kg of CO_2 per kilogram of cement and is responsible for roughly 8% of global anthropogenic greenhouse gas emissions [1], [2]. Hardened Portland cement concrete is also brittle by nature. Its tensile to compressive strength ratio stays below 0.12, and cracks initiate with little post-crack energy absorption [3]. Brittleness is measured here as the brittleness index (BI). This index is defined as the ratio of the 28-day compressive strength to the 28-day modulus of rupture. A high BI increases the cost of tensile reinforcement and limits the structural efficiency of pavements, slabs and shells [4].

Marble dust (MD) is a fine calcium carbonate byproduct of ornamental stone cutting. It acts as an additional supplementary cementitious material through a physical microfilling mechanism. The calcium carbonate content densifies the interface transition zone without pozzolanic reaction [5], [6]. In many studies, the optimum level of ordinary Portland cement substitution has been

determined to be between 5% and 12%. Sathe et al. [7] found a 17% increase in 28-day compressive strength at 5% MD. Agrawal et al. [8] found that a substitution level of 7.5% was optimum under water curing and provided a 9.5% increase in strength. Sai et al. [9] reported an increase in compressive strength by combining 10% MD and polypropylene fiber dosage. Corinaldesi et al. [10] observed a 7.6% increase in strength at 10-12% MD.

Yin et al. [11] reported 15–35% improvements in flexural strength at 0.5–1.0% PP volume ratio. Borg et al. [12] observed an 18–27% increase in flexural toughness at 1.0% rPET volume ratio. Al-Hagri and Döndüren [13] confirmed that rPET fibers reduced compressive strength but increased ductility in the OPC matrix compared to steel fibers. Yazıcı et al. [14] documented monotonic gains in compressive and flexural strength with SF up to 1.0% volume ratio.

This study makes three contributions. It tests PP, rPET, and SF fibers within a single marble-dust-modified matrix. The brittleness index is the primary outcome, measured alongside compressive and flexural strength. Additionally, a cost efficiency index and an environmental efficiency index are introduced.

The program was carried out in three stages. Stage I identified the optimum MD replacement level, from 5% to 14% of binder mass, and a constant water to binder ratio of 0.364. Stages II and III introduced PP (0.25–1.00%), rPET (0.50–1.50%), and SF (0.50–1.75%) into the invariant MD10 matrix, across twelve dosages. Four analytical indices (brittleness index, flexural efficiency ratio, specific strength, and specific flexure) together with an early-age strength prediction model, were used to characterize the mechanical behavior. A cost efficiency index and an environmental efficiency index then bring the economic and environmental comparison together.

2. Materials and Experimental Program

2.1 Parameter Selection

Table 1 summarizes the studies that informed the experimental parameters. Marble dust replacement studies converge on an optimum of 5–12% of binder mass. Stage I therefore tested a 5–14% range, with 10% targeted as the central value. The PP volume-fraction range (0.25–1.00%) covered the optimum reported by Yin et al. [11] and the MD-PP range examined by Sai et al. [9]. The rPET range (0.50–1.50%) addressed the compressive-flexural divergence observed by Al-Hagri and Döndüren [13] and Borg et al. [12]. The SF range (0.50–1.75%) extended through the clustering threshold reported by Yoo et al. [15].

Table 1. Studies informing the experimental design

No.	Reference	Matrix	MD (%)	PP V_f (%)	rPET V_f (%)	SF V_f (%)	Key finding
1	[7]	OPC concrete, w/c 0.45	2.5–20 (opt. 5)	–	–	–	5% MD raised CS_{28} by 17%; denser pore structure at low MD
2	[8]	OPC concrete, multiple curing regimes	2.5–15 (opt. 7.5)	–	–	–	7.5% MD with water curing raised CS by 9.5%
3	[9]	OPC concrete, PCE admixture	0–20 (opt. 10)	0–1.0	–	–	Combined MD and PP addition improved compressive performance near 10% MD
4	[10]	Concrete, constant w/b	10–12	–	–	–	CS_{28} increased by 7.6% at 10–12% MD
5	[11]	Review of 40 PP-FRC studies	–	0.5–1.0 (opt. 0.5)	–	–	Flexural strength improved 15–35% at optimum PP dosage
6	[12]	OPC concrete	–	–	1.0	–	Flexural toughness improved 18–27%; compressive strength reduced 5–14%
7	[13]	OPC concrete,	–	0.5, 1.0	0.5, 1.0	0.5, 1.0	Steel fiber gave best overall performance; PP and PET reduced CS but improved ductility
8	[14]	Steel fiber reinforced concrete	–	–	–	up to 1.0	Monotonic CS and MoR gains with steel fiber up to 1.0%
9	[15]	Ultra-high-performance FRC	–	–	–	0–1.25+	Fiber clustering threshold identified near 1.25%

2.2 Cementitious Materials

CEM I 42.5N cement, conforming to EN 197-1:2011 [18], was supplied by the National Cement Company, Yemen. Marble dust was collected as a dry by-product from the Al-Rohani Marble Factory. The material originated from limestone quarried in the Marib governorate. It was oven-dried for 24 hours and sieved through a No. 270 sieve before use. Table 2 summarizes the chemical and physical properties of the cement and marble dust. X-ray fluorescence analysis showed a calcium oxide content of 64.30 wt.%, consistent with a pure limestone source. The combined reactive oxide content (SiO_2 + Al_2O_3 + Fe_2O_3) was 16.48 wt.%, below the 70 wt.% minimum required by ASTM C618-19 [19] for natural pozzolan classification. The material therefore acts as a non-pozzolanic calcareous filler. It contributes through physical micro-filler action and $CaCO_3$ nucleation rather than pozzolanic reaction [5], [6]. Specific gravity was 2.643.

Table 2. Chemical and physical properties of cement and marble dust

Property / oxide	Unit	OPC	Marble dust
SiO_2	%	21.23	10.05
Al_2O_3	%	5.92	4.53
Fe_2O_3	%	4.05	1.89
CaO	%	57.77	64.30
MgO	%	3.03	2.55
SO_3	%	2.75	—
Chloride content	%	0.01	—
Insoluble residue	%	3.34	—
SiO_2+Al2O_3+Fe2O_3	%	—	16.48
Specific gravity	—	3.15	2.643
Blaine fineness	cm^2/g	3565	—
Initial setting time	min	200	—
Final setting time	min	265	—
Le Chatelier expansion	mm	1.0	—
CS 2d	MPa	23.17	—
CS 7d	MPa	33.59	—
CS 28d	MPa	45.19	—

2.3 Aggregates

Coarse aggregate was crushed basalt from a local quarry. It was supplied in three size fractions (12.5, 9.5, and 4.75 mm) and blended to meet the ASTM C33/C33M [20] grading requirements. The Los Angeles abrasion loss was 14.5%, determined as per ASTM C131 [21]. Specific gravity and water absorption were calculated according to ASTM C127 [22], and their values were 2.879 and 1.26%, respectively. Fine aggregate from the Zagan region was used. Its specific gravity was 2.48, and its fineness modulus was 2.33, as determined by ASTM C128 [23] and ASTM D2419 [24].

A polycarboxylate ether superplasticizer, conforming to EN 934-2 [25], was used at a base dosage of 0.80% by binder mass. This was increased to a maximum of 1.10% for the highest fiber dosages to maintain slump at a constant w/b.

2.4 Fiber Reinforcement

Three fiber types were selected to span the mechanical performance and sustainability range of available reinforcement options. Fiber properties are summarized in Table 3 and Figure 1 show their appearance.

Polypropylene macro-fibers (P) had an embossed rectangular cross-section, length 56 mm, equivalent diameter 1.0 mm (L/d = 56), density 910 kg/m^3, tensile strength 500 MPa, elastic modulus 10 GPa, and embodied carbon 1.58 kg CO_2e/kg [26].

Recycled PET strips (rPET) were manually cut from post-consumer water bottles to length 50 mm, equivalent diameter 0.833 mm (L/d = 60), density 1380 kg/m^3, tensile strength 55 to 80 MPa, elastic modulus 2.1 to 3.1 GPa, and embodied carbon 0.45 kg CO_2e/kg [17].

Hooked-end steel fibers (SF) had length 50 mm, diameter 1.0 mm (L/d = 50), density 7810 kg/m^3, tensile strength 1200 MPa, elastic modulus approximately 200 GPa, and embodied carbon 2.46 kg CO_2e/kg [16].



Figure 1. Fiber types: (a) polypropylene macrofiber; (b) recycled PET strip; (c) hooked-end steel fiber

Table 3. Fiber properties

Property	PP	rPET	SF
Type	Commercial microfiber	Recycled waste strip	Commercial hooked-end wire
Length (mm)	56	50	50
Equivalent diameter (mm)	1.0	0.833	1.0
Aspect ratio, L/d	56	60	50
Density (kg/m^3)	910	1380	7810
Tensile strength (MPa)	500	55–80	1200
Elastic modulus (GPa)	10	2.1–3.1	~200
Surface geometry	Embossed rectangular	Smooth flat strip	Hooked ends
CO_2e (kg/kg)	1.58	0.45	2.46
Price (USD/kg)	1.80	0.05	1.20

2.5 Experimental Program and Mix Design

In this study, the experimental work was conducted in three stages. In the first stage, the effect of marble dust was studied. Six mixes were prepared. A control mix with no MD was included. Five additional mixes were prepared with MD at 5%, 8%, 10%, 12%, and 14% by weight of cement. The 10% MD mix was selected as the base for fiber addition. In the second stage, fibers were added to the MD10 matrix. PP fibers were added at 0.25%, 0.50%, and 1.00% by volume. Recycled PET fibers were also added at 0.50%, 1.00%, and 1.50% in separate mixtures. In the third stage,

SF were added to the MD10 matrix. Six volume fractions were examined: 0.50%, 0.75%, 1.00%, 1.25%, 1.50%, and 1.75%. The complete mixing ratios for all stages are given in Table 4.

Table 4. Mix proportions

Mix ID	OPC (kg/m^3)	MD (kg/m^3)	Basalt (kg/m^3)	Sand (kg/m^3)	Water (kg/m^3)	SP (%)	Fiber (kg/m^3)	V_f (%)	Slump (mm)
Stage I									
CTRL	440.29	0.00	1012.23	657	159.84	0.80	0	0	100
MD5	418.27	22.01	1012.23	657	159.84	0.80	0	0	95
MD8	405.06	35.22	1012.23	657	159.84	0.80	0	0	90
MD10	396.26	44.03	1012.23	657	159.84	0.80	0	0	80
MD12	387.45	52.83	1012.23	657	159.84	0.80	0	0	75
MD14	378.65	61.64	1012.23	657	159.84	0.80	0	0	70
Stage II — PP fibers									
MD10-Ref	396.26	44.03	1012.23	657	159.84	0.80	0	0	80
PP025	396.26	44.03	1012.23	657	159.84	0.80	2.28	0.25	80
PP050	396.26	44.03	1012.23	657	159.84	0.80	4.55	0.50	75
PP100	396.26	44.03	1012.23	657	159.84	0.90	9.10	1.00	75
Stage II — rPET fibers									
rPET050	396.26	44.03	1012.23	657	159.84	0.80	6.90	0.50	80
rPET100	396.26	44.03	1012.23	657	159.84	0.95	13.80	1.00	75
rPET150	396.26	44.03	1012.23	657	159.84	1.10	20.70	1.50	75
Stage III — SF fibers									
SF050	396.26	44.03	1012.23	657	159.84	0.80	39.25	0.50	75
SF075	396.26	44.03	1012.23	657	159.84	0.85	58.88	0.75	75
SF100	396.26	44.03	1012.23	657	159.84	0.90	78.50	1.00	75
SF125	396.26	44.03	1012.23	657	159.84	0.90	98.13	1.25	75
SF150	396.26	44.03	1012.23	657	159.84	0.95	117.75	1.50	75
SF175	396.26	44.03	1012.23	657	159.84	1.00	137.38	1.75	75

2.6 Specimen Preparation and Testing

The same mixing method was followed for all mixtures. The dry materials were mixed for two minutes. Water and superplasticizer were added over three minutes, followed by two minutes of wet mixing. When using fibers, they were added gradually over two minutes to avoid agglomeration. Workability was measured using slump tests according to ASTM C143/C143M [27].

Compressive strength was measured on 100 mm cubes. Testing was carried out at 7 and 28 days. The test procedure followed BS EN 12390-2 [28] and BS EN 12390-3 [29]. Flexural strength was measured on 100 × 100 × 700 mm prisms at 7 and 28 days using four-point loading per ASTM C78/C78M [30]. Three specimens were tested for each property at each age. A total of 228 specimens were cast.

2.7 Analytical Performance Indices

The brittleness index (BI) was used as the main performance indicator. It is defined as the ratio of 28-day compressive strength to 28-day modulus of rupture (Eq. 1). A lower BI means a better balance between compressive and flexural strength. BI is only a comparative measure of brittleness. It does not directly measure post-cracking ductility. That requires load-deflection or toughness data. Plain concrete typically has a BI between 7 and 10 [4], [31]. Fiber-reinforced composites often show BI values of 5 to 6, which indicate quasi-ductile behavior [3].

$$BI = CS_{28} / MoR_{28} \quad (1)$$

The flexural efficiency ratio (FER) is the reciprocal of BI (Eq. 2). It helps explain how BI is reduced. Two pathways are possible. In the first, MoR_{28} increases while CS_{28} increases or stays the same. In the second, CS_{28} decreases while MoR_{28} increases. Both pathways can produce similar BI values. FER, combined with the individual changes in CS_{28} and MoR_{28}, reveals which pathway is active.

$$FER = MoR_{28} / CS_{28} \quad (2)$$

SF are much denser than PP fibers. The density of steel is 7810 kg/m³, while PP is 910 kg/m³. To account for this, specific strength (Eq. 3) and specific flexure (Eq. 4) were calculated. These were normalized by 28-day density (ρ_{28}).

$$Specific\ strength = CS_{28} / \rho_{28} \quad (3)$$

$$Specific\ flexure = MoR_{28} / \rho_{28} \quad (4)$$

2.8 Economic Assessment

Material costs were calculated at the batching plant. Purchase costs were included. Transport, labor, mixing, formwork, and curing were not included. The cost per cubic metre was calculated using Eq. 5. Mass is expressed in kg/m³ and price is expressed in USD/kg.

$$C_{\mathrm{mix}} = \Sigma\,(m_{\mathrm{i}} \times p_{\mathrm{i}}) \quad (5)$$

Prices were based on the Sana'a market. Plain concrete was priced at 80 USD/m³. A full price schedule is given in Table 5. Marble dust and rPET were treated as waste materials. Their prices were set near zero.

The cost efficiency index (CEI) was calculated using Eq. 6. CEI expresses the cost per unit reduction in BI. Lower CEI values indicate more cost-effective brittleness mitigation.

$$CEI = \Delta C_{\mathrm{mix}} / |\,\Delta BI\,| \quad (6)$$

where ΔC_{mix} is the cost difference between a fiber mixture and MD10-Ref, and $|\Delta BI|$ is the magnitude of BI reduction.

Table 5. Unit material prices

Material	Price (USD/kg)	Basis
OPC	0.1203	Calibrated from CTRL mix cost benchmark (80 USD/m^3); consistent with World Bank Yemen cement import data
Marble dust	0.002	Waste by-product; price reflects collection, drying, and sieving labour only
Basalt aggregate	0.015	Local quarry delivered price, Sana'a region
Natural sand	0.010	Local delivered price, Zajan area supply
PP fiber	1.800	SikaFiber-142 regional distributor, mid-range published price
rPET fiber	0.050	Near-zero material cost; price reflects cutting and preparation labour
Steel fiber	1.200	SikaFiber-502 regional distributor, published price range 1.0–1.4 USD/kg
Superplasticizer	1.500	Polycarboxylate ether HRWR, regional admixture market data
Mixing water	0.000	Negligible; excluded from cost calculation

2.9 Environmental Life Cycle Assessment

Environmental impact was evaluated using a cradle-to-gate life cycle approach. The assessment followed ISO 14040 and ISO 14044. The scope covered raw material extraction, transport to processing, and manufacturing. On-site mixing, curing, use, and end-of-life were excluded, consistent with precedent in the fiber-reinforced concrete literature [32], [33].

Embodied carbon per cubic meter was calculated using Eq. 7 as the sum of the product of each constituent mass and its validated cradle-to-gate emission factor:

$$E_{\mathrm{mix}} = \Sigma\,(m_{\mathrm{i}} \times EF_{\mathrm{i}}) \tag{7}$$

where m_i is the mass of constituent i per cubic meter of concrete (kg/m^3), and EF_i is its cradle-to-gate unit emission factor (kg CO_2e/kg).
The adopted OPC emission factor, 0.830 kg CO_2e/kg, accounts for calcination and kiln fuel combustion and is supported by Andrew [1] and the ICE v2.0 database [16]. Andrew [1] reported a calcination contribution of 0.507 kg of CO_2 per kg of clinker based of global cement-production data spanning 1928 to 2018. The rPET factor, 0.45 kg CO_2e/kg, comes from an ISO 14044-compliant assessment of mechanically recycled PET bottles, which reported a 79% reduction relative to virgin PET production (2.15 kg CO_2e/kg) [17]. The PP factor, 1.58 kg CO_2e/kg, comes from a regional life cycle assessment of polypropylene production [26]. The steel fiber factor, 2.46 kg CO_2e/kg, comes from the ICE v2.0 database entry for wire-drawn steel [16]. The cradle to gate emission factors is given in Table 6.

The environmental efficiency index (EEI; Eq. 8) expresses incremental embodied carbon per unit BI reduction:

$$EEI = \Delta E_{\mathrm{mix}} / |\,\Delta BI\,| \tag{8}$$

Here, ΔE_{mix} is the embodied carbon difference between a fiber mixture and MD10-Ref. |ΔBI| is the magnitude of BI reduction. EEI is expressed in kg CO_2e/m^3 per BI unit. Lower values indicate a more carbon-efficient brittleness mitigation strategy.

Table 6. Cradle-to-gate emission factors

Material	EF (kg CO_2e/kg)	Source / basis
OPC	0.830	Andrew [1] and ICE v2.0[16], generic cradle-to-gate OPC factor
Marble dust	0.005	Waste-stream proxy; ICE v2.0 crushed-limestone basis [16]
Basalt aggregate	0.0083	ICE v2.0 crushed-rock factor [16], proxy for local basalt
Natural sand	0.0050	ICE v2.0 general natural-aggregate factor [16], proxy for local sand
PP fiber	1.580	Alsabri et al.[26], GCC-region cradle-to-gate PP resin factor
rPET fiber	0.450	ALPLA/denkstatt [17], mechanically recycled PET factor
Steel fiber (SF)	2.460	ICE v2.0 wire-drawn steel [16], supported by World Steel Association LCI [34]
Superplasticiser	2.200	MECLA [45], generic polycarboxylate-ether proxy
Mixing water	0.000	Negligible; excluded per standard LCA practice

3. Results

3.1 Marble Dust Replacement Level

The results of Stage I are presented in Table 7 and Figure 2. The CS_{28} increased from 45.13 MPa in the control mix to 49.64 MPa at 10% MD. It then decreased to 45.92 MPa at 12% MD and to 43.23 MPa at 14% MD. The relationship followed a parabolic trend. In the upward segment (0–10% MD), the strength increased by 0.454 MPa per 1% MD. In the downward segment (10–14% MD), the strength decreased by 0.603 MPa per 1% MD. The decline was steeper than the increase.

The MoR_{28} followed the same trend. it increased from 5.76 MPa to 6.18 MPa at a 10% MD (+7.3%). After that decreased to 5.24 MPa at a 14% MD. The loss of flexural strength (-15.2%) was greater than the loss of compressive strength (-12.9%). This indicates a greater sensitivity of the flexural properties to clinker dilution.

The compressive strength after 7 days showed the same parabolic pattern. This confirms that the microfilling mechanism is active from the early age. MD10 was chosen as the reference matrix because it achieved the highest values for both CS_{28} and MoR_{28}. It also reduced material costs and had a low carbon content within the tested ratios.

Table 7. Stage I mechanical results

Mix ID	MD (%)	ρ_{28} (kg/m^3)	CS_{7d} (MPa)	CS_{28d} (MPa)	MoR_{7d} (MPa)	MoR_{28d} (MPa)	ΔCS_{28} (%)
CTRL	0	2431.33	31.10	45.13	4.40	5.76	—
MD5	5	2431.26	32.62	47.18	4.58	5.90	+4.5%
MD8	8	2437.50	33.88	48.67	4.65	5.98	+7.8%
MD10	10	2445.69	35.47	49.64	4.96	6.18	+10.0%
MD12	12	2436.90	33.54	45.92	4.50	5.56	+1.7%
MD14	14	2425.27	31.95	43.23	4.32	5.24	−4.2%

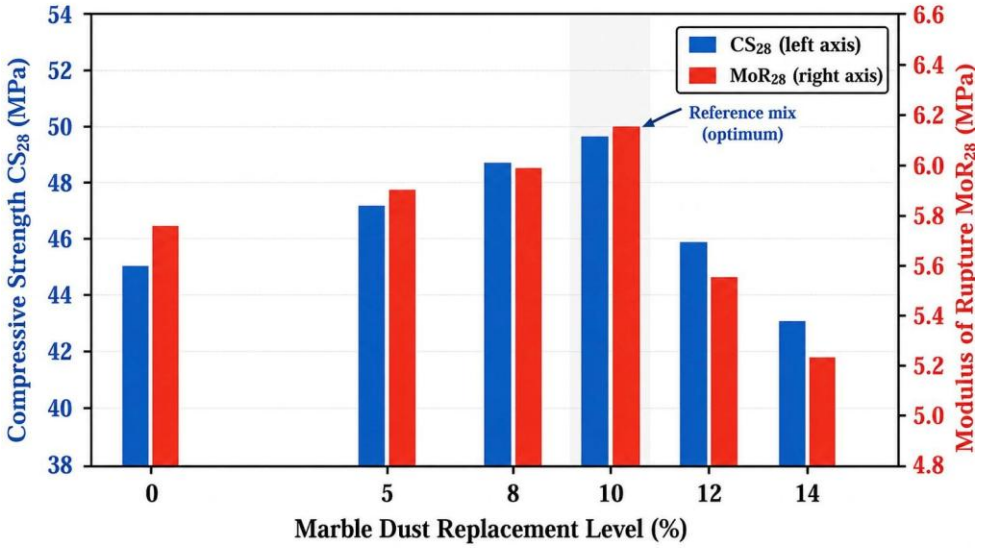


Figure 2. Effect of marble dust replacement level on CS_{28} and MoR_{28}

3.2 Density

PP fibers showed a gradual decrease in density with increasing dosage (figure 3). The density decreased from 2440.13 kg/m³ at 0.25% to 2431.33 kg/m³ at 1.00%. This corresponds to the decreasing density of the PP particles (910 kg/m³) as they are replaced by denser materials.

rPET fibers showed a similar downward trend, despite having a higher density (1380 kg/m³) than PP. The largest decrease in density was recorded at 1.50% for rPET fibers, at 2429.09 kg/m³. SF fibers reversed this trend. The density increased steadily from 2486.77 kg/m³ at 0.50% to 2554.92 kg/m³ at 1.75%.

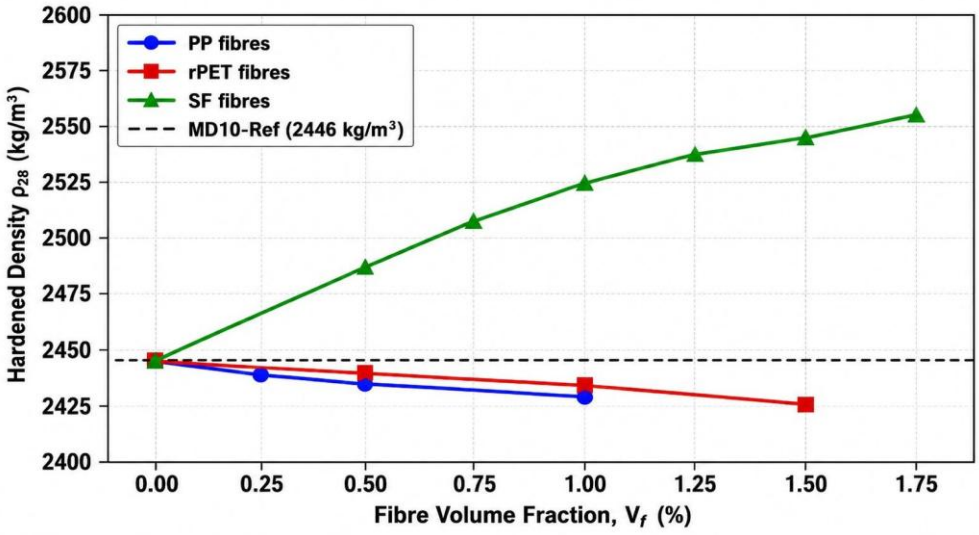


Figure 3. Density vs. fiber volume fraction

3.3 Compressive Strength

Table 8 is summarizing the mechanical properties of the tested samples. As figure 4 shows, In PP mixtures, the CS_{28} increased from 49.64 MPa (MD10-Ref) to a peak of 53.68 MPa at 0.50% (+8.1%). After that it decreased to 50.98 MPa at 1.00% (+2.7%). However, in rPET series, the CS_{28} increased to 51.93 MPa at 0.50% (+4.6%). This trend is similar to PP but with a lower value. It then declined to 45.44 MPa at 1.00% (-8.5%), and then to 42.99 MPa at 1.50% (-13.4%). At 1.50%, CS_{28} was 4.7% lower than the plain control sample (45.13 MPa).

The SF series produced the largest and most consistent gains. CS_{28} increased from 55.10 MPa at 0.50% (+11.0%) to a maximum of 58.74 MPa at 1.25% (+18.3%). It then declined to 55.26 MPa at 1.75% (+11.3%). A positive gain of at least 11% was sustained across the full dosage range. The 7-day compressive strength of SF mixtures (43.94 to 47.03 MPa) exceeded both polymer fiber series at all dosages. This indicates that the confinement contribution of steel fibers is active before 7 days. Figure 6 shows the failure of some tested samples.

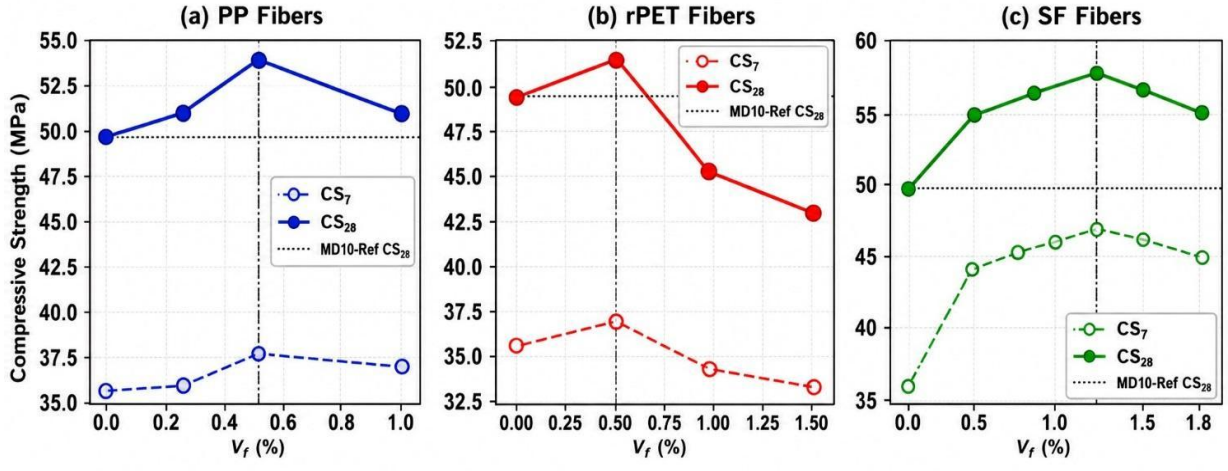


Figure 4. CS_7 and CS_{28} vs. fiber volume fraction for PP, rPET, and SF

3.4 Modulus of Rupture

All three fiber types improved MoR_{28} relative to the reference at every dosage tested (Figure 5). PP fibers peaked at 7.58 MPa at 0.50% (+22.7%). This flexural gain was nearly three times the concurrent compressive gain (+8.1%) at the same dosage. rPET fibers reached 7.78 MPa at 1.00% (+25.9%). This was the highest modulus of rupture among the two polymer fiber types. It occurred at the dosage where compressive strength had already fallen 8.5% below the reference. SF fibers reached a maximum of 9.66 MPa at 1.25% (+56.3%). This flexural gain was more than three times the corresponding compressive gain (+18.3%). Fiber reinforcement improved flexural response across all mixtures, regardless of compressive performance.

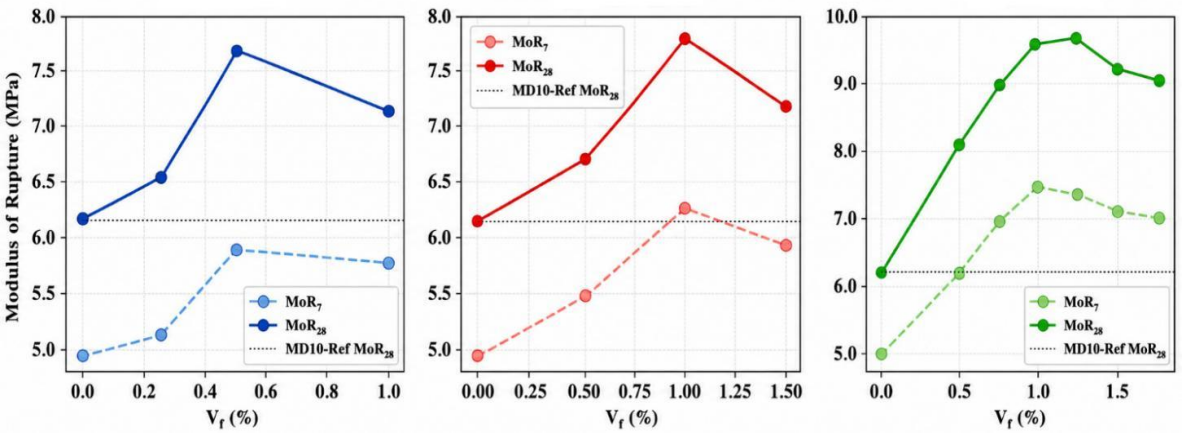


Figure 5. MoR_7 and MoR_{28} vs. fiber volume fraction for PP, rPET, and SF

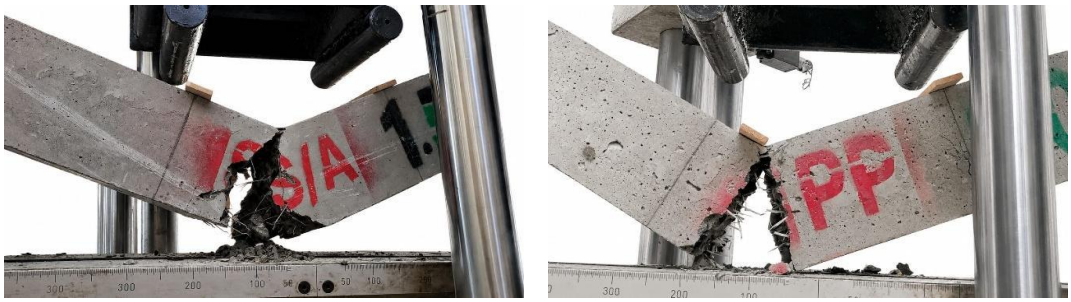


Figure 6. Flexural failure of (a) SF and (b) PP specimens

3.5 Compressive-Flexural Trajectory

The relationship between compressive and flexural strength is shown in Figure 7. Three distinct patterns were observed.

In the SF series, both features increased together. The trajectory moved north-east up to a volume ratio of 1.25%. Subsequently, both features decreased to 1.50% and 1.75%. Clustering is the likely cause of this decline.

The PP series followed a similar northeast arc. Both properties peaked at 0.50% and declined at 1.00%. The clustering threshold for PP is lower than for steel. This explains the earlier reversal.

The rPET series showed a different behavior. From the reference to rPET050, both properties moved northeast together. At rPET100 and rPET150, the trajectory turned northwest. Compressive strength fell below the reference. Flexural strength continued to rise. This reversal was specific to rPET and was not seen with PP or SF.

The trajectory plot reveals more than individual bar charts. It shows the direction of mechanical change and the dosage window of additivity. Steel fibers offer the widest window of simultaneous enhancement, up to 1.25%. PP offers a narrower window, up to 0.50%. rPET offers a trade-off at higher dosages, where flexural gain is obtained at the cost of compressive strength.

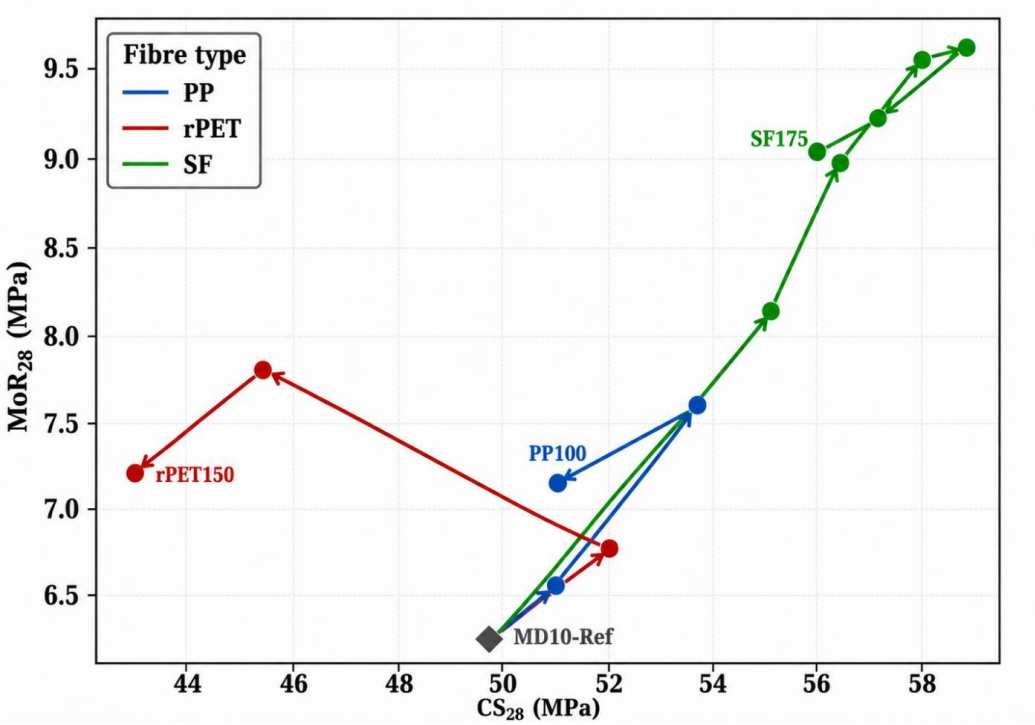


Figure 7. CS_{28} to MoR_{28} trajectory by fiber type

3.6 Brittleness Index and Flexural Efficiency Ratio

As Figure 8 illustrates, all fiber types reduced BI relative to the MD10-Ref value of 8.032 is required to distinguish. Within the PP series, BI fell to a minimum of 7.082 at 0.50% (−11.8%), a numerator-driven reduction in which the relative MoR_{28} gain (+22.7%) substantially outpaced the relative CS_{28} gain (+8.1%) at the same dosage. The rPET series achieved the largest BI reduction recorded, 5.841 at 1.00% (−27.3%). This rPET minimum is a denominator-driven reduction, CS_{28} declined faster in relative terms than MoR_{28} rose, and the corresponding FER of 0.171 is the highest recorded across all fiber-reinforced mixtures, confirming the disproportionate flexural dominance that underlies the rPET brittleness result.

The SF series achieved a minimum of BI = 6.049 at 1.00% (−24.7%) before rising marginally to BI = 6.081 at 1.25% (−24.3%), the dosage that otherwise delivers the series' peak absolute CS_{28} and MoR_{28} values. The near-identical BI values at SF100 and SF125 (6.049 against 6.081, a difference of only 0.53%) despite a considerably larger difference in absolute MoR_{28} between the two dosages (9.58 against 9.66 MPa) illustrates that BI, as a ratio, can remain nearly stationary

even while absolute performance continues to improve, reinforcing the case for reporting BI alongside, rather than instead of, the raw strength values from which it derives.

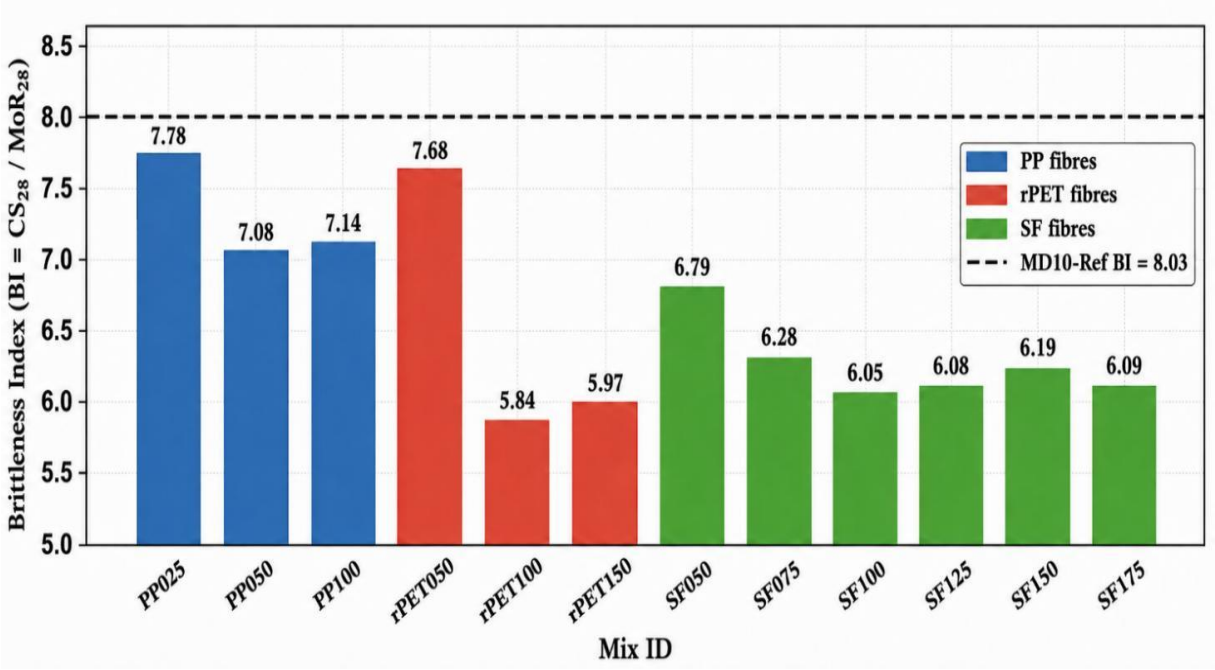


Figure 8. Brittleness index for fiber reinforced mixtures

3.7 Specific Strength and Specific Flexure

Density normalization is necessary for fair cross-fiber comparison. SF increases density, while PP and rPET reduce it. Part of SF's absolute strength advantage is therefore due to additional mass, not efficiency.

In compression, specific strength peaked at SF125 (23.146×10^{-3} MPa·m³/kg). The 18.3% CS_{28} gain at this dosage exceeded the 3.8% density increase by a factor of nearly five. The SF125 compressive advantage therefore remained intact after normalization. PP050 achieved the second-highest specific strength (22.033×10^{-3}) with a density change of only −0.23%. On a weight-normalized basis, PP050 was the most efficient compressive option among the twelve mixtures. rPET100 specific strength (18.651×10^{-3}) fell below the MD10-Ref value (20.297×10^{-3}). This confirms that its compressive penalty is real and not a density artifact. Weight normalization does not recover the loss. rPET100 is therefore unsuitable when specific compressive performance governs the design.

In the flexural dimension, specific flexure revealed a result not apparent from absolute MoR_{28} values. rPET100 (3.193×10^{-3} MPa·m³/kg) exceeded PP050 (3.111×10^{-3}) in specific flexure. Their absolute MoR_{28} values were similar (7.78 vs. 7.58 MPa). Their densities were also near-identical (2436.29 vs. 2436.31 kg/m³). The small MoR advantage of rPET100 was therefore preserved after density normalization.

For applications governed by flexural performance per unit self-weight, rPET100 is the most weight-efficient polymer fiber solution identified in this study. This applies to thin precast slabs, lightweight panels, and composite shells.

SF dominated specific flexure at all dosages, with values from 3.265 to 3.806 × 10^{-3}. SF125 recorded the maximum (3.806 × 10^{-3}). Even after accounting for the self-weight penalty of steel, its flexural advantage over both polymer types remained substantial.

3.8 Early-Age Strength Prediction

The early-age prediction model is explained in Eq. 9 (Figure 9). A single set of regression coefficients applies across all three fiber types:

$$CS_{28} = 19.585 + 0.826 \times CS_7 \quad (R^2 = 0.853) \tag{9}$$

The R^2 value of 0.853 means that CS_7 alone explains 85.3% of CS_{28}. This is true even though the three fiber types have different CS_7 values. Fiber type does not change the maturity pathway. It only changes the final strength.

A slope coefficient of 0.826 indicates a relatively faster maturation in the SF series. For SF mixtures, CS_7 represents 85–90% of CS_{28}. For MD10-Ref and PP mixtures, CS_7 represents approximately 71% of CS_{28}. This difference reflects the early-age confinement contribution of steel fibers.

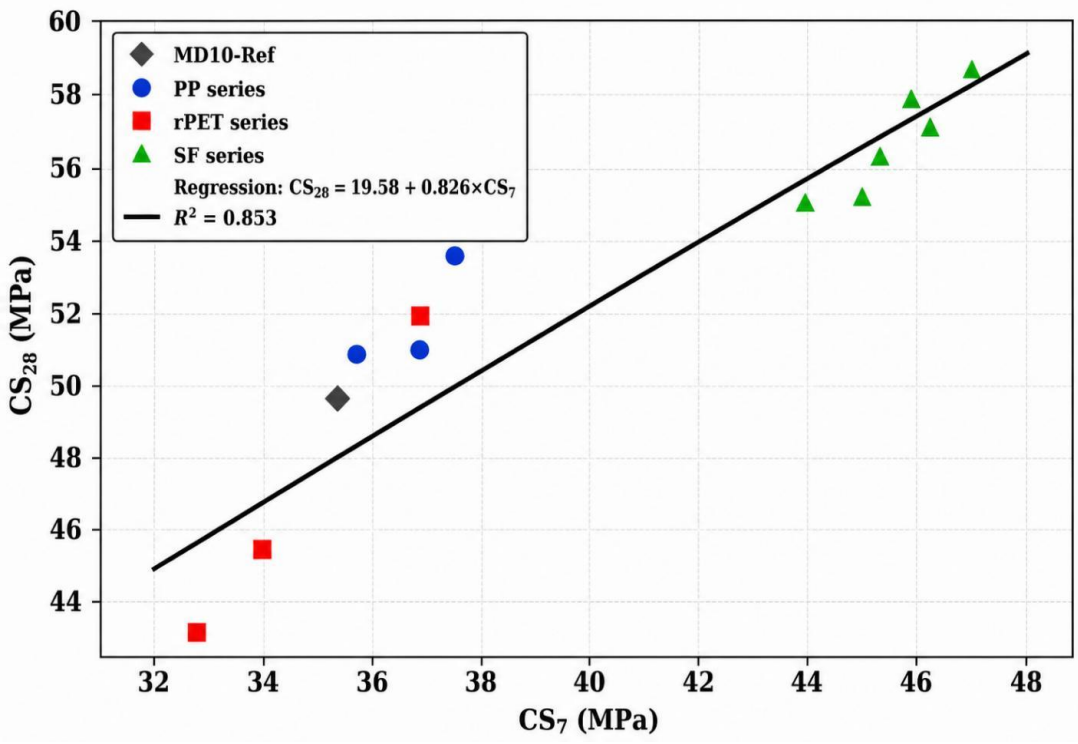


Figure 9. Empirical correlation between CS_7 and CS_{28}

3.9 Material Cost and Embodied Carbon

The full economic and environmental assessment is summarized in Table 9. Figure 10 shows that the MD10-Ref baseline cost 74.79 USD/m^3 and carried 348.55 kg CO2e/m^3, reductions of 6.5% and 9.4% respectively relative to the plain OPC control (80.00 USD/m^3; 384.87 kg CO2e/m^3), confirming that the 10% marble dust substitution alone delivers a measurable economic and

environmental benefit before any fiber is introduced. OPC accounted for 94.4% of MD10-Ref embodied carbon (328.90 of 348.55 kg CO_2e/m3), against a marble dust contribution of only 0.22 kg CO_2e/m3 despite its 44.03 kg/m^3 mass share of the binder, reflecting the roughly 166-fold difference between the OPC and marble dust emission factors (0.830 against 0.005 kg CO_2e/kg).

Among the fiber series, rPET produced by far the smallest cost and carbon increments at every dosage tested, 0.35 USD/m^3 and 3.10 kg CO_2e/m^3 at 0.50%, rising only to 1.68 USD/m^3 and 7.66 kg CO_2e/m^3 at 1.00%, keeping the entire three-dosage rPET series below both the cost and the embodied carbon of the plain OPC control. PP050 added a moderate 8.19 USD/m^3 and 7.19 kg CO_2e/m^3, remaining affordable relative to its mechanical gain. SF produced by far the largest increments of any fiber type, rising from 47.10 USD/m^3 and 96.55 kg CO_2e/m^3 at 0.50% to 118.42 USD/m^3 (+158% relative to MD10-Ref) and 242.36 kg CO_2e/m3 (+69.5%) at 1.25%, where steel fiber alone accounted for 69.3% of total mixture embodied carbon, displacing OPC as the dominant emissions source at that dosage, a reversal not observed at any dosage of either polymer fiber type.

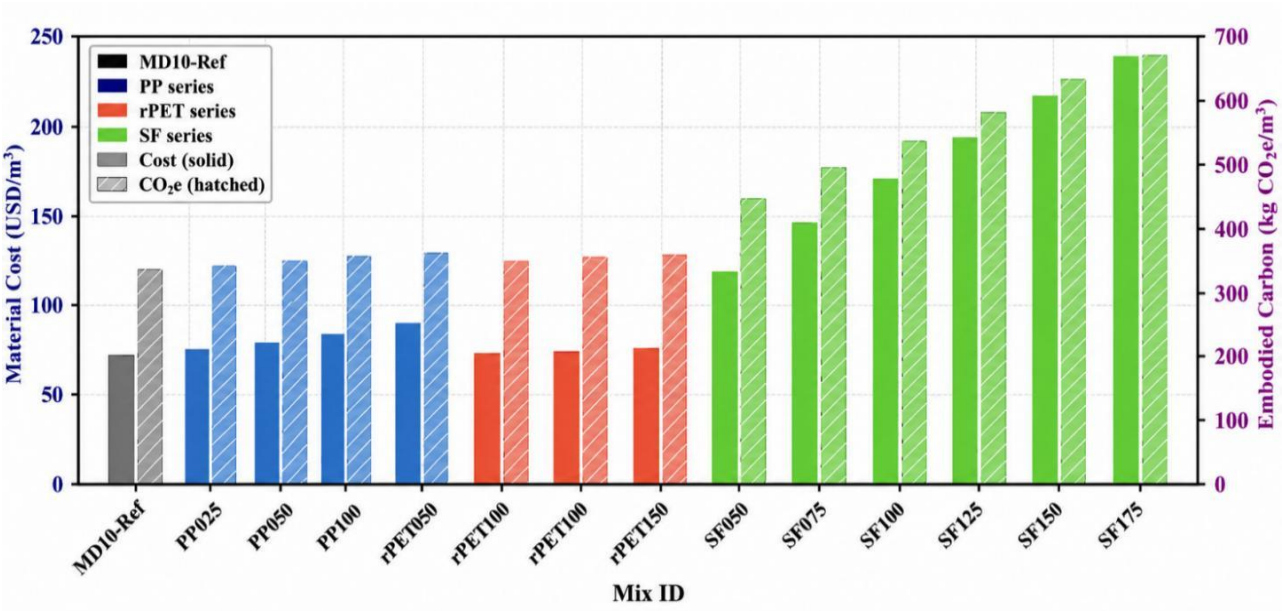


Figure 10. Material cost and embodied carbon by mixture

3.10 Cost and Environmental Efficiency

The cost and carbon increments were normalized by the BI reduction achieved by each mixture (Figure 11). This reframes the mechanical results from Sections 3.3 to 3.6 in terms of economic and environmental cost per unit of brittleness improvement.

rPET100 recorded the minimum values for both indices: CEI = 0.77 USD/m³ per BI unit and EEI = 3.50 kg CO_2e/m³ per BI unit. This means each unit reduction in BI corresponds to 0.77 USD/m³ of additional material cost and 3.50 kg CO_2e/m³ of additional embodied carbon. rPET050 was the second most efficient mixture, with CEI = 0.98 and EEI = 8.86. It remained an order of magnitude more cost-efficient than any SF dosage.

PP050 recorded CEI = 8.62 and EEI = 7.57. It was approximately eleven-fold less cost-efficient than rPET100, despite comparable carbon efficiency. This divergence reflects PP's higher unit

price (1.80 USD/kg) relative to its emission factor (1.58 kg CO_2e/kg), compared to rPET's near-zero values (0.05 USD/kg; 0.45 kg CO_2e/kg).

The SF series recorded the highest CEI and EEI values at all dosages. Values ranged from CEI = 37.78 and EEI = 77.45 at 0.50% to CEI = 85.37 and EEI = 174.62 at 1.75%. The latter represents a 79-fold higher cost and 36-fold higher carbon intensity than rPET100 per unit of BI reduction.

A higher CEI or EEI at a given SF dosage does not indicate an inferior system in absolute terms. SF125 still delivers the largest numerator-driven BI reduction through simultaneous dual enhancement and the highest absolute MoR_{28} recorded.

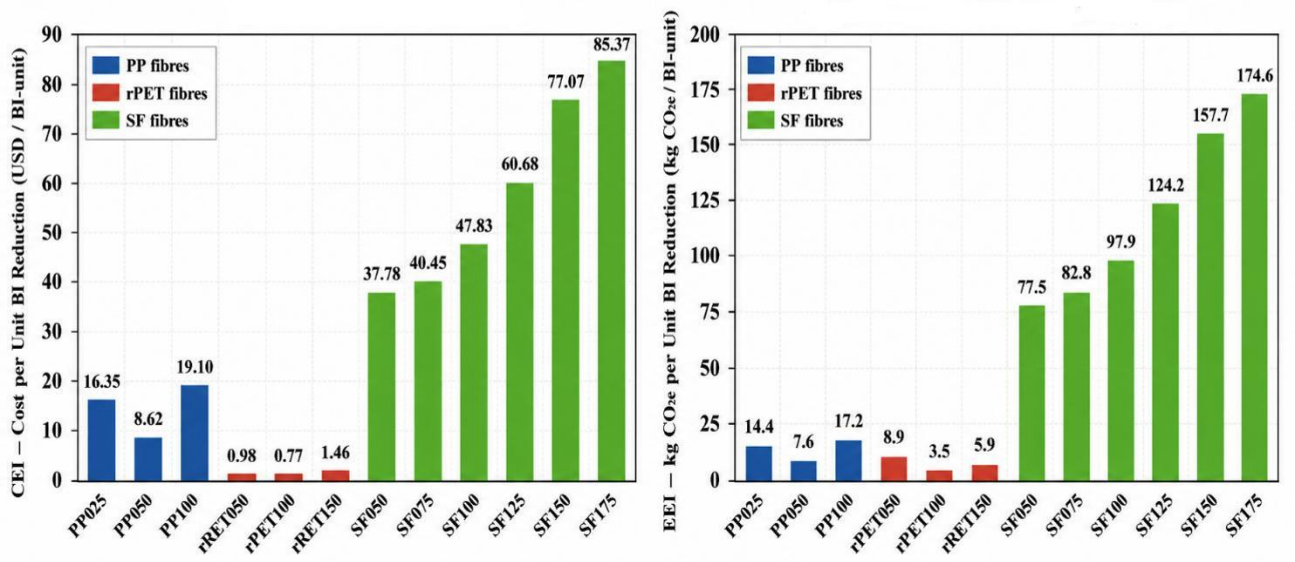


Figure 11. Cost efficiency index and environmental efficiency index by mixture

3.11 Multi-Criterion Comparison

A radar comparison was carried out for the three optimal mixtures. PP at 0.50%, rPET at 1.00%, and SF at 1.25% were compared against the MD10-Ref baseline. The results are presented in Figure 12. The baseline was set to 1.0 on all six axes. The axes were CS_{28}, MoR_{28}, ductility (1/BI), specific flexure, FER, and specific strength.

The largest total closed area was observed for SF125. The CS_{28} and MoR_{28} vertices extended significantly. Gains of 18.3% and 56.3% were recorded, respectively. Specific flexure was maximized. The FER vertex extended only slightly beyond the reference.

A well-proportioned, quasi-symmetric profile was shown by PP050. Each vertex extended beyond the baseline. No deficiency was observed on any axis. This reflects the selective nature of PP reinforcement. MoR_{28} was raised disproportionately. CS_{28} was raised slightly. Density remained essentially unchanged.

The most asymmetric profile was exhibited by rPET100. The highest ductility (1/BI) and FER vertex were recorded for this mixture. However, the CS_{28} vertex was clearly compressed within the reference hexagon. The specific strength vertex also fell below the baseline.

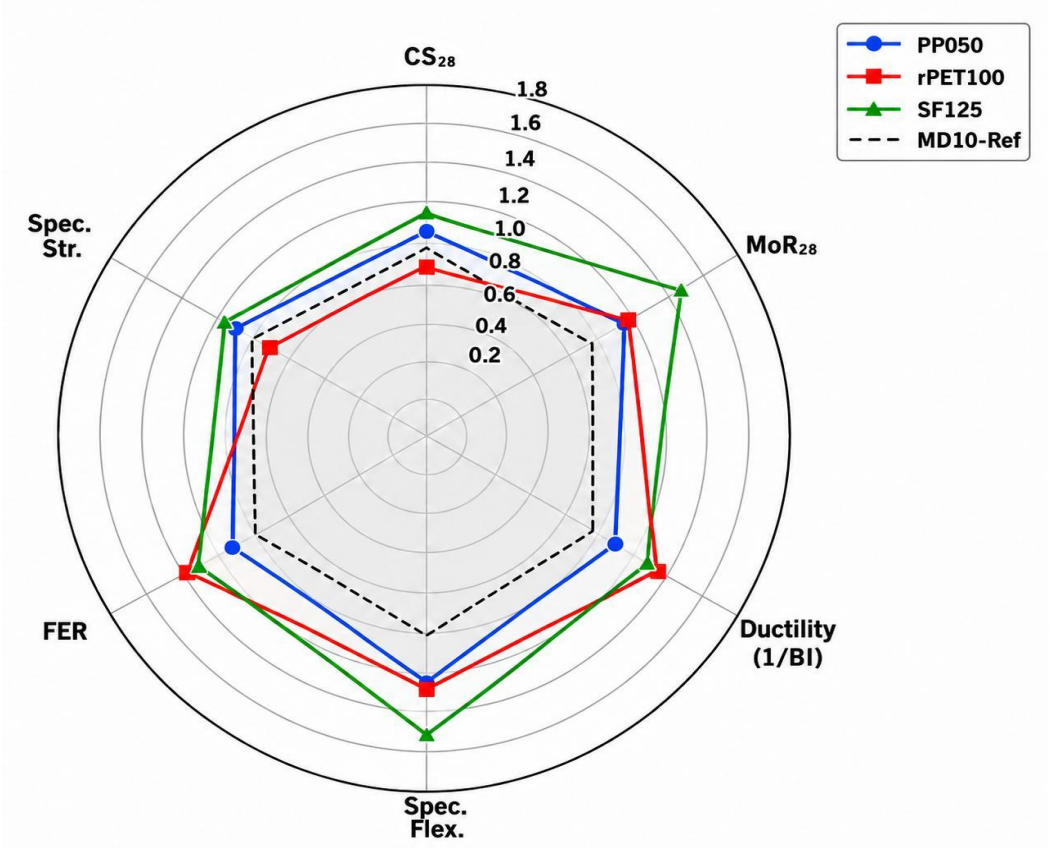


Figure 12. Multi-criterion radar comparison of optimal mixtures

Table 8. Mechanical properties results

Mix	Fiber	V_f (%)	ρ_{28} (kg/m^3)	CS_7 (MPa)	CS_{28} (MPa)	ΔCS_{28} (%)	MoR_7 (MPa)	MoR_{28} (MPa)	ΔMoR_{28} (%)	BI	FER	Sp. Str. ($\times10^{-3}$)	Sp. Flex. ($\times10^{-3}$)
MD10-Ref	-	0	2445.69	35.47	49.64	-	4.96	6.18	-	8.032	0.124	20.297	2.527
PP025	PP	0.25	2440.13	35.72	50.89	+2.5%	5.16	6.54	+5.8%	7.781	0.129	20.855	2.680
PP050	PP	0.50	2436.31	37.53	53.68	+8.1%	5.90	7.58	+22.7%	7.082	0.141	22.033	3.111
PP100	PP	1.00	2431.33	36.89	50.98	+2.7%	5.78	7.14	+15.5%	7.140	0.140	20.968	2.937
rPET050	rPET	0.50	2441.03	36.89	51.93	+4.6%	5.52	6.76	+9.4%	7.682	0.130	21.274	2.769
rPET100	rPET	1.00	2436.29	34.04	45.44	−8.5%	6.30	7.78	+25.9%	5.841	0.171	18.651	3.193
rPET150	rPET	1.50	2429.09	32.78	42.99	−13.4%	5.98	7.20	+16.5%	5.971	0.167	17.698	2.964
SF050	SF	0.50	2486.77	43.94	55.10	+11.0%	6.18	8.12	+31.4%	6.786	0.147	22.157	3.265
SF075	SF	0.75	2507.51	45.28	56.37	+13.6%	6.95	8.98	+45.3%	6.277	0.159	22.480	3.581
SF100	SF	1.00	2524.34	45.92	57.95	+16.7%	7.44	9.58	+55.0%	6.049	0.165	22.956	3.795
SF125	SF	1.25	2537.85	47.03	58.74	+18.3%	7.35	9.66	+56.3%	6.081	0.165	23.146	3.806
SF150	SF	1.50	2545.01	46.23	57.16	+15.1%	7.10	9.24	+49.5%	6.186	0.162	22.460	3.631
SF175	SF	1.75	2554.92	44.97	55.26	+11.3%	7.04	9.08	+46.9%	6.086	0.164	21.629	3.554

Table 9. Economic and environmental assessment

Mix	Cost (USD/m³)	CO_2e (kg/m³)	BI	Δcost (USD/m³)	ΔCO_2e (kg/m³)	CEI (USD·m⁻³/BI unit)	EEI (kg CO_2e·m⁻³/BI unit)
MD10-Ref	74.79	348.55	8.032	—	—	—	—
PP025	78.90	352.15	7.781	+4.10	+3.60	16.35	14.35
PP050	82.98	355.74	7.082	+8.19	+7.19	8.62	7.57
PP100	91.83	363.89	7.140	+17.04	+15.35	19.10	17.20
rPET050	75.14	351.65	7.682	+0.35	+3.10	0.98	8.86
rPET100	76.47	356.21	5.841	+1.68	+7.66	0.77	3.50
rPET150	77.81	360.77	5.971	+3.02	+12.22	1.46	5.93
SF050	121.89	445.10	6.786	+47.10	+96.55	37.78	77.45
SF075	145.78	493.88	6.277	+70.99	+145.33	40.45	82.80
SF100	169.65	542.62	6.049	+94.86	+194.07	47.83	97.86
SF125	193.21	590.91	6.081	+118.42	+242.36	60.68	124.19
SF150	217.08	639.66	6.186	+142.29	+291.11	77.07	157.68
SF175	240.97	688.44	6.086	+166.18	+339.89	85.37	174.62

4. Discussion

4.1 Marble Dust Optimum

The optimum of Stage I was found at 10% MD. A 10.0% increase in CS_{28} and a 7.3% increase in MoR_{28} was recorded. These values are within the range reported in the marble powder literature. Aliabdo et al. [6] reported a 9.4% increase in CS_{28} at 10% MD in cement mortar cured under standard conditions. This value closely matches the compressive increase observed in the present study. Corinaldesi et al. [10] reported a 7.6% CS_{28} gain at 10 to 12% MD replacement in concrete at constant w/b. Sathe et al. [7] identified a lower optimum, 5% MD, with a considerably larger gain of 17%, in a higher w/c system (0.45); the higher water content in that system likely amplifies the relative contribution of micro-filler densification to the pore structure, shifting the optimum toward a lower replacement level before dilution effects dominate. Agrawal et al. [8] found the compressive optimum shifts to 7.5% under water curing specifically, with a 9.5% gain, indicating that curing regime modulates the optimum replacement level in addition to w/b.

The mechanistic framework proposed by Vardhan et al. [5], interfacial transition zone (ITZ) densification through $CaCO_3$ nucleation of C-S-H combined with physical void filling by sub-53-micrometre MD particles, explains both the existence of an optimum and its approximate location. Below the optimum, the available MD surface area is insufficient to fully densify the ITZ, so the densification benefit is under-realized. Above the optimum, the same mechanism runs in reverse. Clinker dilution reduces the C_3S and C_2S available for long-term calcium silicate hydrate formation, and while $CaCO_3$ can react with aluminate phases to form carboaluminate hydrates, this reaction does not compensate volumetrically for the lost C-S-H gel [6], [36]. The results show

this reversal is asymmetric. A modest 1.7% CS_{28} gain remains at 12% MD, whereas the system falls 4.2% below the plain control at 14%, This decline is steeper decline than the near-linear loss reported by Topcu et al. [36] in self-compacting MD concrete, suggesting that the w/b = 0.364 matrix used here reaches the dilution-dominated regime more abruptly than higher-w/b systems.

4.2 Polypropylene Fiber Behavior

The PP compressive response was inverted-parabolic. It peaked at 0.50% (+8.1%) and retreated at 1.00% (+2.7%). The flexural gain at 0.50% was +22.7%. These results agree with the findings of Yin et al. [11]. Flexural gains of 15–35% were reported at 0.5–1.0% PP. The flexural gain here was at the lower end of that range. This is attributed to the MD10 matrix, which was already densified.

PP acts through crack arrest at the micro-crack stage [37]. At low dosage, both CS_{28} and MoR_{28} are raised. The flexural gain exceeds the compressive gain. This reflects the mode-selectivity of fiber bridging. Bending isolates a single crack. Compression involves distributed cracking. Fibers are therefore more efficient in bending [3].

The maturity ratio (CS_{28}/CS_7) was unchanged by PP addition. Values ranged from 1.42 to 1.43, similar to the MD10-Ref value of 1.40. PP is chemically inert and does not alter hydration kinetics.

The decline at 1.00% is due to fiber balling. The clustering threshold for polyolefin fibers is 0.50–0.75% [35]. Above this, fiber clusters form weak zones and crack initiation sites. Performance therefore declines.

4.3 Recycled PET Fiber Behavior

The most significant finding in the rPET series was the compressive-flexural divergence. At 1.00% volume fraction, CS_{28} fell by 8.5% while MoR_{28} rose by 25.9%. This divergence is larger than in most prior studies.

In compression, load transfer depends on adhesion between the fiber and the matrix. The PET surface is smooth and hydrophobic. A weak bond is formed with the cement paste [40]. Voids and poor wetting were observed at the interface by Behzadian and Shahrajabian [40]. This explains the compressive strength loss.

In bending, the mechanism is different. Crack propagation across a single plane is governed by fiber count and geometry, not bond quality. The rPET aspect ratio (L/d = 60) is higher than PP (56) and SF (50). At the same volume fraction, more rPET fibers cross the crack plane. Each fiber provides frictional pull-out resistance. The combined effect is a substantial bridging force, even without strong adhesion [39], [41].

The BI at rPET100 was 5.841. This was lower than any SF dosage. Brittleness mitigation is therefore not proportional to absolute mechanical performance. This finding agrees with Borg et [12], who reported a flexural toughness advantage for rPET. The present results extend their work by quantifying the trade-off through the FER decomposition.

4.4 Steel Fiber Behavior

The SF series was the only fiber type that raised both CS_{28} and MoR_{28} simultaneously. This dual enhancement was sustained up to 1.25% volume fraction. This finding is consistent with Yazıcı et al. [14], who reported the same pattern up to 1.0%. The present results extend the peak to 1.25%.

Under compression, the mechanism is passive confinement. The steel fiber network intercepts splitting cracks. This is analogous to hoop reinforcement [42]. The confinement increases both compressive strength and ductility.

Under bending, the hooked ends provide anchorage. As the crack widens, the anchorage engages and sustains load transfer. This effect is stronger than smooth fiber pull-out [43].

The decline beyond 1.25% is due to fiber clustering. Fiber-fiber contact increases non-linearly at high volume fractions. Agglomerations displace paste and form weak planes [15], [44]. The superplasticizer dosage was adjusted from 0.80% to 1.00% to maintain workability. This only partially offset the clustering at the highest dosages.

4.5 Economic Trade-offs

The MD10-Ref basic model is 6.5% cheaper than plain OPC control. This saving is achieved before any fiber is added. This is because marble powder has almost zero cost (0.002 USD/kg), replacing a proportional amount of OPC (0.1203 USD/kg). Among fiber types, rPET fiber achieves the lowest cost increase per dosage. PP is in the mid-range, while steel (SF) fiber is in the highest. This ranking is based on unit price and mass dosage. rPET costs US$0.05/kg, while SF costs US$1.20/kg; this represents a 24-fold difference. Mass dosage is directly proportional to fiber density, and therefore has the highest density for steel (7810 kg/m³). When normalized by BI reduction, rPET100 is the most cost-efficient brittleness mitigator. It achieves a CEI of 0.77 USD/m³ per BI unit. This is because it represents a larger reduction in BI (2,191 units from 8,032 to 5,841) and a smaller increase in cost (USD 1.68/m³) compared to any SF dosage.

4.6 Environmental Trade-offs

Embodied carbon results reflected cost findings. MD10-Ref had 9.4% less embodied carbon than plain concrete. This is because MD's emission factor (0.005 kg CO_2e/kg) is lower compared to OPC (0.830 kg CO_2e/kg).

The embodied carbon of rPET at 1.00% remained lower than that of plain concrete. However, in SF at 1.25% exceeded the reference level by 70%. Steel fibers alone contributed 69% of total emissions at this dosage. This is due to the high mass and carbon density of the fibers. SF has 2.46 kg CO_2e/kg. rPET has 0.45 kg CO_2e/kg. This is a 5.5-fold difference.

For every reduction in the BI, rPET was 36 times more carbon-efficient than SF. This is consistent with published studies. Habert et al.[32] showed that steel fiber contributes disproportionately to carbon emissions.

4.7 Structural Selection Guidance

The results point to a fiber-selection framework. The framework is organized by the governing structural criterion. It complements, not replaces, code-based design (ACI 318-19 [47], fib Model Code [48]).

For compression-governed members (columns, shear walls, pile caps), SF at 1.25% is preferred. It gives the highest CS_{28} with favorable CEI and EEI. PP at 0.50% is a secondary option if steel is unavailable. rPET above 0.50% is unsuitable if compressive class requirements are binding. CS_{28} falls below MD10-Ref from rPET100 onward.

For flexure-governed members (slabs, pavements, precast elements), the choice depends on the criterion.

Where absolute MoR governs (AASHTO [50]), SF at 1.00–1.25% is preferred. SF100 (9.58 MPa) and SF125 (9.66 MPa) are close substitutes.

Where the fib Model Code residual strength ratio are controlled [48], rPET at 1.00% is preferred. This requires compressive demand below 45.44 MPa.

Where self-weight is binding (seismic ASCE 7-22 [51]), PP at 0.50% or rPET at 1.00% are preferred. Both add negligible density.

In constructions where cost and carbon emissions are controlled, MD10 with rPET at 1.00% is the best option.

5. Conclusions

In this study, the potential for reducing brittleness using PP, recycled PET, and hooked-end steel fibers in a marble dust-modified concrete matrix was evaluated. Mechanical tests were combined with cost and carbon efficiency assessments. The main key findings are summarized as follows:

- For 10% MD was used, the CS_{28} and MoR_{28} values increased by 10.0% and 7.3%, respectively. Whereas, the material costs and carbon emissions decreased by 6.5% and 9.4%, respectively, when compared to plain concrete.
- Polypropylene fiber with a 0.50% volume fraction provided an 11.8% reduction in brittleness, without changing hydration kinetics at all dosages tested.
- The use of 1.00% by volume of recycled PET fibers resulted in the greatest reduction in brittleness (27.3%), thanks to a denominator-dependent approach that combines the disadvantage of compression with a large gain in flexural strength.
- Steel fibers with a volumetric ratio of 1.25% produced the highest absolute compressive and flexural strengths (18.3% and 56.3% respectively) through true double reinforcement, with performance decreasing after this dose due to fiber agglomeration.
- The cost efficiency index and environmental efficiency index identify recycled PET fiber as the dominant strategy where efficiency, rather than absolute performance, governs fiber selection, at 79-fold lower cost and 36-fold lower carbon intensity than the optimal steel-fiber dosage per unit of brittleness reduction.

- An early-age prediction model (CS_{28} = 19.585 + 0.826 x CS_7, R^2 = 0.853) applies across all three fiber types within the MD10 matrix.

Future work should priorities splitting tensile testing to extend the brittleness assessment to direct tension, microstructural analysis of the rPET-paste interface to confirm the proposed bonding mechanism, surface treatment of rPET to recover compressive performance, durability testing of the optimal mixtures under chloride and sulphate exposure, and evaluation of hybrid rPET-SF systems at sub-optimal individual dosages.

CRediT Authorship Contribution Statement

Ibrahim Alameri: Conceptualization, Methodology, Writing – original draft, Supervision. Abdulmalek Al-Jolahy: Investigation, Formal analysis, Data curation. Ali A. Al-Kadas: Investigation, Validation, Writing – review and editing. Abdulwahed A. Mohmmed: Methodology, Resources. Sulaiman Alsafi: Investigation, Visualization.

Funding

This research did not receive any specific grant from funding agencies in the public, commercial, or not-for-profit sectors.

Declaration of Competing Interest

The authors declare that they have no known competing financial interests or personal relationships that could have appeared to influence the work reported in this paper.

Data Availability Statement

No. dataset was used.

References

[1] R. M. Andrew, "Global CO 2 emissions from cement production," *Earth System Science Data*, vol. 10, no. 1, pp. 195–217, 2018, doi: 10.5194/essd-2017-77.

[2] P. Monteiro, *Concrete: microstructure, properties, and materials*. McGraw-Hill Publishing, 2006.

[3] A. Bentur and S. Mindess, *Fiber reinforced cementitious composites*. CRC press, 2006. Accessed: Jun. 17, 2026.

[4] P. J. Hannant, "Fiber cements and fiber concretes," 1978. Accessed: Jun. 17, 2026. [Online]. Available: https://trid.trb.org/View/87018

[5] K. Vardhan, S. Goyal, R. Siddique, and M. Singh, "Mechanical properties and microstructural analysis of cement mortar incorporating marble powder as partial replacement of cement," *Construction and Building Materials*, vol. 96, pp. 615–621, 2015, doi: 10.1016/j.conbuildmat.2015.08.071.

[6] A. A. Aliabdo, M. Abd Elmoaty, and E. M. Auda, "Re-use of waste marble dust in the production of cement and concrete," *Construction and building materials*, vol. 50, pp. 28–41, 2014, doi: 10.1016/j.conbuildmat.2013.09.005.

[7] S. Sathe, S. Patil, and Y. N. Bhosale, "Investigation of strength, durability, and microstructure properties of concrete with waste marble powder as a partial replacement of cement," *World Journal of Engineering*, vol. 23, no. 1, pp. 71–81, 2026, doi: 10.1108/WJE-06-2024-0372.

[8] N. Agrawal, S. Rashid, M. Singh, A. Srivastava, and R. Khapre, "Marble dust as a sustainable cementitious material: investigating the synergistic effects of curing conditions," *European Journal of Environmental and Civil Engineering*, vol. 29, no. 12, pp. 2472–2494, Sep. 2025, doi: 10.1080/19648189.2025.2492064.

[9] A. N. Sai, M. Sakthivel, G. K. Arunvivek, P. Kumar, R. Dharmaraj, and R. Y. Sembeta, "Mechanical and durability assessment of marble dust-fiber concrete supported by ML prediction," *Scientific reports*, vol. 16, no. 1, Dec. 2026, doi: 10.1038/s41598-026-40874-z.

[10] V. Corinaldesi, G. Moriconi, and T. R. Naik, “Characterization of marble powder for its use in mortar and concrete,” *Construction and building materials*, vol. 24, no. 1, pp. 113–117, 2010, doi: 10.1016/j.conbuildmat.2009.08.013.
[11] S. Yin, R. Tuladhar, F. Shi, M. Combe, T. Collister, and N. Sivakugan, “Use of macro plastic fibers in concrete: A review,” *Construction and Building Materials*, vol. 93, pp. 180–188, 2015, doi: 10.1016/j.conbuildmat.2015.05.105.
[12] R. P. Borg, O. Baldacchino, and L. Ferrara, “Early age performance and mechanical characteristics of recycled PET fiber reinforced concrete,” *Construction and Building Materials*, vol. 108, pp. 29–47, 2016, doi: 10.1016/j.conbuildmat.2016.01.029.
[13] M. G. Al-Hagri and M. S. Döndüren, “Effect of single and hybrid incorporation of steel, polypropylene, and PET fibers on the properties of concrete under static and impact loading,” 2025, doi: 10.1680/jmacr.24.00401.
[14] Ş. Yazıcı, G. İnan, and V. Tabak, “Effect of aspect ratio and volume fraction of steel fiber on the mechanical properties of SFRC,” *Construction and Building Materials*, vol. 21, no. 6, pp. 1250–1253, 2007, doi: 10.1016/j.conbuildmat.2006.05.025.
[15] D.-Y. Yoo, S.-T. Kang, and Y.-S. Yoon, “Effect of fiber length and placement method on flexural behavior, tension-softening curve, and fiber distribution characteristics of UHPFRC,” *Construction and Building materials*, vol. 64, pp. 67–81, 2014, doi: 10.1016/j.conbuildmat.2014.04.007.
[16] G. P. Hammond and C. I. Jones, “Embodied energy and carbon in construction materials,” *Proceedings of the institution of civil engineers-energy*, vol. 161, no. 2, pp. 87–98, 2008, doi: 10.1680/ener.2008.161.2.87.
[17] “Study confirms the excellent carbon footprint of recycled PET | ALPLA Blog.” Accessed: Jun. 18, 2026. [Online]. Available: https://blog.alpla.com/en/press-release/newsroom/study-confirms-excellent-carbon-footprint-recycled-pet/08-17?utm_source=chatgpt.com
[18] B. EN, “197-1: 2011.(2011). EN 197-1cements,” *British Standard Institute*.
[19] ASTM International and ASTM C618, “Standard Specification for Coal Ash and Raw or Calcined Natural Pozzolan for Use in Concrete.” Accessed: Jul. 22, 2026. [Online]. Available: https://store.astm.org/c0618-25a.html
[20] ASTM International and ASTM C33/C33M-24, “Standard Specification for Concrete Aggregates.” Accessed: Jul. 22, 2026. [Online]. Available: https://webstore.ansi.org/standards/astm/astmc33c33m24
[21] ASTM International and ASTM C131/C131M, “Standard Test Method for Resistance to Degradation of Small-Size Coarse Aggregate by Abrasion and Impact in the Los Angeles Machine.”
[22] ASTM International and ASTM C127-24 -, “Standard Test Method for Relative Density (Specific Gravity) and Absorption of Coarse Aggregate.”
[23] ASTM C128-22, “Standard Test Method for Relative Density (Specific Gravity) and Absorption of Fine Aggregate.” Accessed: Jul. 22, 2026. [Online]. Available: https://store.astm.org/c0128-22.html
[24] “Standard Test Method for Sand Equivalent Value of Soils and Fine Aggregate.” Accessed: Jul. 22, 2026. [Online]. Available: https://store.astm.org/d2419-22.html
[25] “A polycarboxylate ether (PCE)-based high-range water-reducing admixture was used. According to the manufacturer’s datasheet, the product complies with EN 934-2, Tables 11.1 and 11.2.” ADIUM-132.
[26] A. Alsabri, F. Tahir, and S. G. Al-Ghamdi, “Life-cycle assessment of polypropylene production in the gulf cooperation council (GCC) region,” *Polymers*, vol. 13, no. 21, p. 3793, 2021, doi: 10.3390/polym13213793.
[27] ASTM International, ASTM C143/C143M-20, and M. International, “Standard Test Method for Slump of Hydraulic-Cement Concrete,” ASTM Philadelphia, PA, USA, 2020.
[28] British Standards Institution and BS EN 12390-7:2019, “Testing hardened concrete Density of hardened concrete,” https://www.en-standard.eu. Accessed: Jul. 23, 2026. [Online]. Available: https://www.en-standard.eu/bs-en-12390-7-2019-testing-hardened-concrete-density-of-hardened-concrete/
[29] British Standards Institution and BS EN 12390-3:2019, “Testing hardened concrete Compressive strength of test specimens.” Accessed: Jul. 22, 2026. [Online]. Available: https://www.en-standard.eu/bs-en-12390-3-2019-testing-hardened-concrete-compressive-strength-of-test-specimens/
[30] ASTM C78/C78M-22, “Standard test method for flexural strength of concrete (using simple beam with third-point loading).” American Standards Testing Materials, 2022. doi: 10.1520/C0078_C0078M-22.
[31] *Report on the physical properties and durability of fiber-reinforced concrete*. American Concrete Institute, 2010.
[32] G. Habert, C. Billard, P. Rossi, C. Chen, and N. Roussel, “Cement production technology improvement compared to factor 4 objectives,” *Cement and concrete research*, vol. 40, no. 5, pp. 820–826, 2010, doi: 10.1016/j.cemconres.2009.09.031.

[33] N. Tošić, J.-M. Torrenti, T. Sedran, and S. Lapičević, “Toward life cycle assessment of concrete: Background data and environmental impacts of ordinary Portland cement production in Serbia.,” *Road Materials and Pavement Design*, vol. 22, no. 5, pp. 1168–1186, 2021, doi: 10.1080/14680629.2019.1696058.
[34] World Steel Association, “Life Cycle Inventory Study Report: 2021 Data Release,” World Steel Association, Brussels, Belgium, 2022.
[35] M. G. Alberti, A. Enfedaque, J. C. Gálvez, and V. Agrawal, “Fiber distribution and orientation of macro-synthetic polyolefin fiber reinforced concrete elements,” *Construction and Building Materials*, vol. 122, pp. 505–517, 2016, doi: 10.1016/j.conbuildmat.2016.06.083.
[36] I. B. Topcu, T. Bilir, and T. Uygunoğlu, “Effect of waste marble dust content as filler on properties of self-compacting concrete,” *Construction and building Materials*, vol. 23, no. 5, pp. 1947–1953, 2009, doi: 10.1016/j.conbuildmat.2008.09.007.
[37] S. Kakooei, H. M. Akil, M. Jamshidi, and J. Rouhi, “The effects of polypropylene fibers on the properties of reinforced concrete structures,” *Construction and Building Materials*, vol. 27, no. 1, pp. 73–77, 2012, doi: 10.1016/j.conbuildmat.2011.08.015.
[38] F. Pelisser, O. R. K. Montedo, P. J. P. Gleize, and H. R. Roman, “Mechanical properties of recycled PET fibers in concrete,” *Materials Research*, vol. 15, no. 4, pp. 679–686, Jul. 2012, doi: 10.1590/S1516-14392012005000088.
[39] S. B. Kim, N. H. Yi, H. Y. Kim, J.-H. J. Kim, and Y.-C. Song, “Material and structural performance evaluation of recycled PET fiber reinforced concrete,” *Cement and concrete composites*, vol. 32, no. 3, pp. 232–240, 2010, doi: 10.1016/j.cemconcomp.2009.11.002.
[40] R. Behzadian and H. Shahrajabian, “Experimental study of the effect of nano-silica on the mechanical properties of concrete/PET composites,” *KSCE Journal of Civil Engineering*, vol. 23, no. 8, pp. 3660–3668, 2019, doi: 10.1007/s12205-019-2440-9.
[41] F. Fraternali, I. Farina, C. Polzone, E. Pagliuca, and L. Feo, “On the use of R-PET strips for the reinforcement of cement mortars,” *Composites Part B: Engineering*, vol. 46, pp. 207–210, 2013, doi: 10.1016/j.compositesb.2012.09.070.
[42] B. Sabariman, A. Soehardjono, W. Wisnumurti, A. Wibowo, and T. Tavio, “Stress-Strain Behavior of Steel Fiber-Reinforced Concrete Cylinders Spirally Confined with Steel Bars,” *Advances in Civil Engineering*, vol. 2018, no. 1, p. 6940532, Jan. 2018, doi: 10.1155/2018/6940532.
[43] M. C. Nataraja, N. Dhang, and A. P. Gupta, “Stress–strain curves for steel-fiber reinforced concrete under compression,” *Cement and concrete composites*, vol. 21, no. 5–6, pp. 383–390, 1999, doi: 10.1016/S0958-9465(99)00021-9.
[44] S. Grunewald, “Performance-based design of self-compacting fiber reinforced concrete,” 2004, Accessed: Jun. 18, 2026. [Online]. Available: https://research.tudelft.nl/en/publications/performance-based-design-of-self-compacting-fiber-reinforced-conc-2/
[45] M. Hsie, C. Tu, and P. S. Song, “Mechanical properties of polypropylene hybrid fiber-reinforced concrete,” *Materials Science and Engineering: A*, vol. 494, no. 1–2, pp. 153–157, 2008, doi: 10.1016/j.msea.2008.05.037.
[46] M. Nili and V. Afroughsabet, “Combined effect of silica fume and steel fibers on the impact resistance and mechanical properties of concrete,” *International journal of impact engineering*, vol. 37, no. 8, pp. 879–886, 2010, doi: 10.1016/j.ijimpeng.2010.03.004.
[47] ACI Committee 318, “Building Code Requirements for Structural Concrete and Commentary (ACI 318-19 and ACI 318R-19), Farmington Hills, MI: American Concrete Institute, 2019.,” American Concrete Institute, 2019.
[48] Fédération Internationale du Béton, *fib model code for concrete structures 2010*. John Wiley & Sons, 2013.
[49] A. W. Beeby and R. S. Narayanan, *Designers’ Guide to EN 1992-1-1 Eurocode 2: Design of Concrete Structures: General Rules and Rules for Buildings and Structural Fire Design*, vol. 17. Thomas Telford, 2005. Accessed: Aug. 11, 2026. [Online]. Available: https://books.google.com/books?hl=en&lr=&id=9Ua7KKD-4FEC&oi=fnd&pg=IA3&dq=EN+1992-1-1&ots=7q9-A4jt1_&sig=5AOzo1w__CTkERtyWr8ZJ74YcvU
[50] T. Officials, “AASHTO guide for design of pavement structures,” *Transportation Officials: Washington, DC, USA*, 1993.
[51] A. 7-22, “Minimum Design Loads and Associated Criteria for Buildings and Other Structures,” ASCE Virginia, USA, 2022.